科学通报 2026 年 第 71 卷 第 25 期: 6107 ~ 6114
论 文
《中国科学》杂志社
SCIENCE CHINA PRESS

化学气相沉积法制备二维碱金属稀土硒化物单晶

张佳麟[1], 陈晓慧[2], 林立[2*], 李春虎[1*]

1. 中国海洋大学化学化工学院, 海洋化学理论与工程技术教育部重点实验室, 青岛 266100
2. 北京大学材料科学与工程学院, 北京 100871
* 联系人, E-mail: linli-cnc@pku.edu.cn; lichunhu@ouc.edu.cn

2025-08-14 收稿, 2025-10-23 修回, 2025-10-24 接受, 2025-10-28 网络版发表

摘要 近年来, 二维材料因其在极限薄厚度下表现的优异物理化学性质而被广泛关注. $NaYbSe_2$因其作为量子自旋液体候选材料和在高压下表现出超导特性而成为研究热点. 然而, 目前仍没有系统制备二维$NaYbSe_2$的相关报道. 本研究以重稀土元素金属加氯化钠可控硒化为技术路线, 通过化学气相沉积法, 以NaCl、Yb和Se作为前驱体, 使用氢气与氩气作为载气, 成功在R< 1$\bar{1}$0 2>面蓝宝石衬底上制备出了二维$NaYbSe_2$材料. 通过调控生长参数, 可以制备15~89 nm不同厚度的纳米片, 进一步表征结果证实$NaYbSe_2$纳米片具有良好的单晶特性. 此制备方法可以进一步拓展至$NaLuSe_2$、$KYbSe_2$和$KLuSe_2$一系列二维单晶薄片的合成. 因此, $NaYbSe_2$等二维材料的可控制备与表现出的优异单晶特性, 将推动此类碱金属稀土硒化物材料的物性研究与其在自旋器件领域的应用.

关键词 二维材料, 化学气相沉积法, 碱金属稀土硒化物, 单晶

自2004年单层石墨烯成功制备以来[1], 二维材料因其独特的物理化学性质, 以及在电子[2]、光电[3]、自旋电子器件[4]、催化[5]等领域的广阔应用前景而备受瞩目. 迄今为止, 已经成功制备出多种二维材料, 包括石墨烯[6,7]、六方氮化硼[8,9]、过渡金属硫族化合物[10~12]和氧化物[13~15]等. 二维稀土材料凭借其稀土元素独特的局域4f电子和强磁各向异性, 可用于构建高度稳定的纳米磁体, 在自旋电子学器件中展现出巨大的应用潜力; 此外, 其在超导领域可利用界面效应调控邻近体系的超导性能, 为研究新型超导态提供了平台. $NaYbSe_2$因其作为量子自旋液体(quantum spin liquid, QSL)候选材料和在高压下表现出的超导特性, 近年来也受到科学家的重视, 成为未来电子自旋器件重要的候选材料之一. Anderson于1973年[16]提出QSL这一新型的量子物态, 引起了很大的关注. 随后, Anderson等人[17,18]在1987年又进一步提出通过对QSL进行掺杂可实现高温超导的理论. 这一理论引发了科研人员对$NaYbSe_2$由绝缘态向金属态和超导态转变的深入研究. 实验表明, 随着压力的增加, $NaYbSe_2$发生从绝缘态向金属态转变[19~22]. 同时值得注意的是, 有研究表明, 当压力加到26.9 GPa时, $NaYbSe_2$出现超导转变, 表现出零电阻输运行为, 其超导转变温度(T_c)约为5.6 K[23]. 然而, 另有研究表明, $NaYbSe_2$在压力超过103.4 GPa以上时才出现超导性, T_c约为8 K[24]. 总之, 现阶段对于$NaYbSe_2$超导电性行为的研究及其超导机制仍需进一步探索. 此外, 对于$NaYbSe_2$磁性的研究也取得了重要进展. 研究人员在外部磁场为1 T的条件下, 测量了$NaYbSe_2$的磁化率随温度的变化, 结果未观察到磁相变, 表明该材料在2 K以上没有出现长程磁有序性或自旋玻璃态, 而是呈现出动态自旋与准静态自旋共存的特殊状态. 据此提出了“铁磁滴浸润在量子自旋液体海洋中的混合态”模型, 即$NaYbSe_2$的基态并非纯粹的量

引用格式: 张佳麟, 陈晓慧, 林立, 等. 化学气相沉积法制备二维碱金属稀土硒化物单晶. 科学通报, 2026, 71: 6107–6114
Zhang J, Chen X, Lin L, et al. Chemical vapor deposition growth of two-dimensional alkali-metal-based rare-earth selenide single crystals (in Chinese). Chin Sci Bull, 2026, 71: 6107–6114, doi: 10.1360/CSB-2025-5357

© 2025《中国科学》杂志社

子自旋液体，而是由局域化的短程铁磁团簇嵌入自旋液体共同构成. 这一结果不仅揭示了其复杂的磁响应机制，也为理解量子自旋液体在无序和缺陷环境中的演化提供了新的视角[25]. 同类型的$KYbSe_2$也是一个接近QSL临界点的模型材料，研究人员在实验中同时观测到高度量子纠缠与分数化激发，为量子自旋液体的实验验证提供了关键证据[26~28]. 因此，这类碱金属稀土化合物在量子自旋液体领域扮演着重要角色.

目前，$NaYbSe_2$制备方法如下：使用金属Yb、Se以及NaCl作为助熔剂生长，并且合成的$NaYbSe_2$均为块体材料[20,25]，尚未有二维薄层$NaYbSe_2$成功合成的报道. 众所周知，当块体材料减薄至原子级尺度，会在极限薄的厚度下表现出一些不同于体相的物理化学特性. 例如，MoS_2块体带隙为1.2 eV，发光微弱，而单层MoS_2带隙为1.8 eV，具有高效的光致发光和电致发光特性，适用于制作纳米尺度的发光二极管和激光器. 类似地，$NaYbSe_2$作为一种莫特绝缘体，当其减薄至二维极限时，可能展现出更加显著的电子关联效应和量子涨落行为，从而改变绝缘-金属转变的临界条件，甚至在低压条件下出现新的超导相变. 此外，二维$NaYbSe_2$与石墨烯等高迁移率二维材料构筑异质结后，有望通过层间电荷转移和界面耦合调控其量子态，为探索自旋液体特性、界面诱导超导以及关联电子体系等新奇物理现象提供新的实验平台. 因此，二维$NaYbSe_2$的合成具有重要意义. 本研究在众多可控硒化合成Cr_2Se_3[29]、Fe_7Se_8[30]、CoSe[29]、VSe_2[31]、$PtSe_2$[32]和MnSe[33]等硒化物的基础上，发展了以NaCl、Yb和Se为前驱体，通过化学气相沉积法(chemical vapor deposition, CVD)合成高质量二维$NaYbSe_2$单晶纳米片的方法. 此合成方法可进一步拓展至二维$NaLuSe_2$、$KYbSe_2$和$KLuSe_2$单晶纳米片的合成. 通过精确控制生长条件，制备了不同厚度的二维$NaYbSe_2$单晶，并采用多种表征方法充分证明二维单晶的合成. 本工作为二维$NaYbSe_2$材料的低维物性研究和基于此材料的自旋器件构筑提供了可能.

1 实验

1.1 材料合成

本工作采用化学气相沉积法在双温区管式炉(OTF-1200X-II)中制备出高质量$NaYbSe_2$单晶纳米片. 将硒粉(Se，纯度99.9%，Innochem)放置在上游温区中心，氯化钠(NaCl，纯度99.5%，Aladdin)和金属镱(Yb，纯度99.9%，Aladdin)放置在石英舟中，石英舟置于下游温区中心，选用R< 1$\bar{1}$0 2>面蓝宝石(单面抛光)作为生长衬底，抛光面朝下放置在Yb和NaCl前驱体的上方. 生长开始前使用500 sccm氩气清洗管路10 min，除去管式炉中的残余氧气和水分，后经实验证实管路残存氧气和水分会严重影响生长结果. 生长阶段使用氩气氢气混合气体(Ar 1450 sccm，H_2 50 sccm)作为载气，左右温区间距为10 cm，上游温区设置为400℃，下游温区设置为900℃，升至目标温度后保温20 min开始自然降温，降温至500℃打开炉体，进行快速降温，炉体温度100℃以下取出样品，全程气体流量保持不变. 使用与上述相同方法以Se粉、KCl和Yb为前驱体可制备出$KYbSe_2$单晶；以Se粉、NaCl和Lu为前驱体可制备出$NaLuSe_2$单晶；以Se粉、KCl和Lu为前驱体可制备出$KLuSe_2$单晶.

1.2 材料转移

首先，将聚甲基丙烯酸甲酯(polymethyl methacrylate, PMMA, 950 K A4, Microchem corp)以1000 r/min的转速旋涂到生长有$NaYbSe_2$纳米片的R面蓝宝石衬底表面，并在150℃热台上加热5 min使得胶层固化. 之后，使用热释放胶带(thermal release tape，TRT；编号3198ms，日东电工株式会社)通过辊压机以2 cm/s的速度压合到PMMA表面. 随后，揭下热释放胶带，通过机械力将TRT/PMMA/$NaYbSe_2$复合层从R面蓝宝石衬底上分离，并将剥离下来的材料辊压贴合至SiO_2/Si衬底. 最后，120℃加热释放TRT，并使用丙酮去除PMMA胶层，氮气吹干后获得转移后的$NaYbSe_2$纳米片.

1.3 材料表征

使用光学显微镜(optical microscope, OM, LV150N, Nikon)和原子力显微镜(atomic force microscope, AFM, Dimension Icon, Bruker)对$NaYbSe_2$、$KYbSe_2$、$NaLuSe_2$和$KLuSe_2$四种材料进行形貌和厚度分析. 使用X射线衍射仪(X-ray diffractometer, XRD, D8 ADVANCE, Bruker)和透射电子显微镜(transmission electron microscope, TEM, Tecnai G2 F20, FEI)对上述四种材料的结构进行表征. 通过激光共聚焦拉曼光谱仪(Raman, LabRAM HR-800, Horiba)表征四种材料的拉曼光谱. 进一步使用高角环形暗场扫描透射显微镜(high-angle annular dark-field scanning transmission election microscope, HAADF-STEM, Titan Cubed Themis G2, FEI)观察

$KLuSe_2$ [100]方向的原子排布.

2 结果与讨论

2.1 二维$NaYbSe_2$晶体的晶体结构、合成和表征

$NaYbSe_2$属于三方晶系，R$\bar{3}$m空间群，晶格参数为$a = b = 4.07$ Å, $c = 20.77$ Å[34]. 钠离子位于[$YbSe_6$]八面体层间, $NaYbSe_2$的整体结构由一层Na^+和一层[$YbSe_2$]$^-$组成, 图1(a)是$NaYbSe_2$的晶体结构示意图. 从c轴方向观察, 金属离子Na^+和Yb^{3+}通过与Se^{2-}离子的连接形成类似六方结构. 本研究采用化学气相沉积法成功制备了二维$NaYbSe_2$晶体, 生长示意图如图1(b)所示. 生长

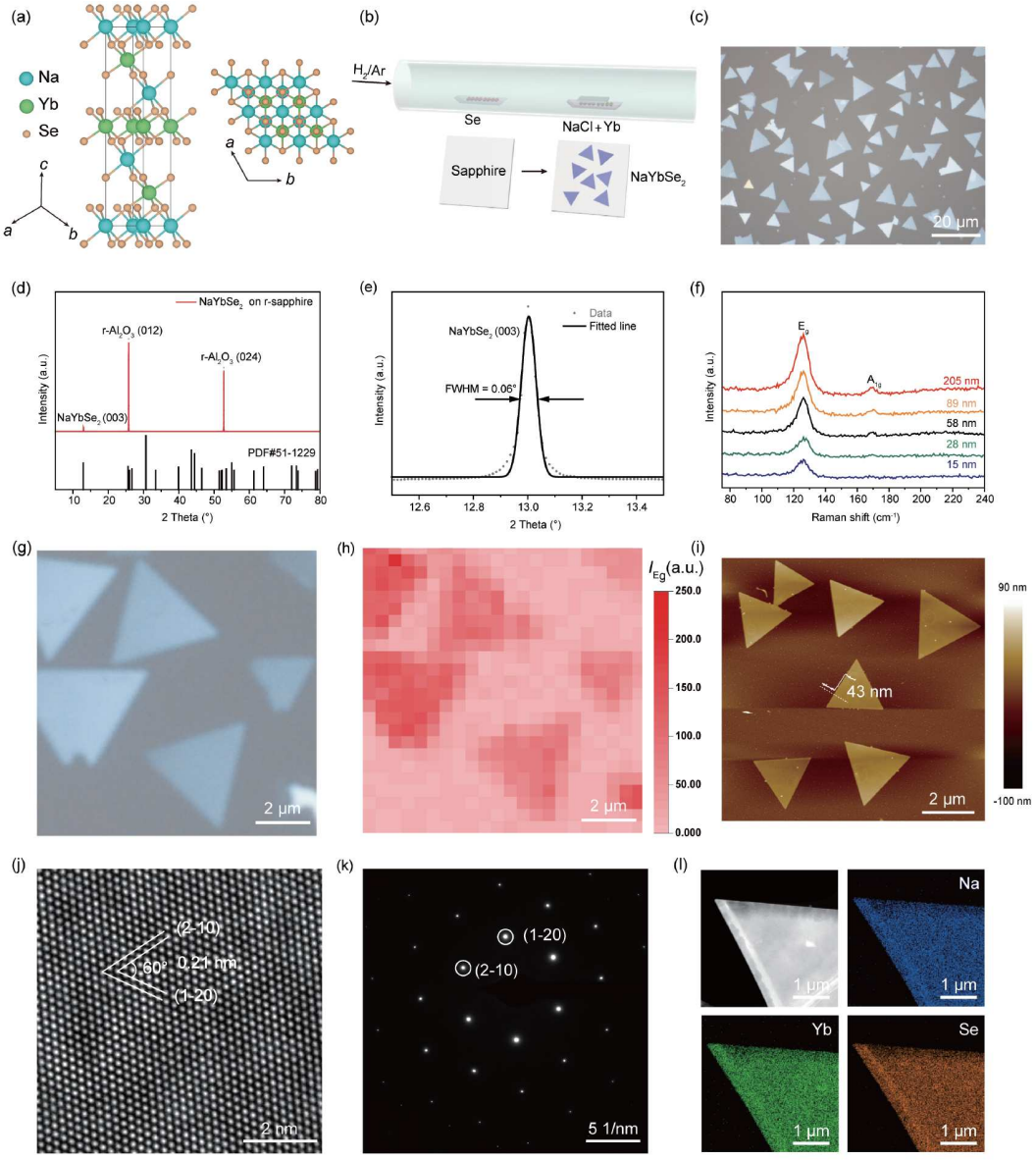


图 1 (网络版彩色)二维$NaYbSe_2$合成及表征. (a) $NaYbSe_2$晶体结构. (b) CVD生长示意图. (c) $NaYbSe_2$的光学照片. (d) XRD测试. (e) $NaYbSe_2$的(003)晶面衍射峰的半峰宽. (f) 不同厚度$NaYbSe_2$的Raman测试. (g, h) $NaYbSe_2$的光学照片和对应的Raman mapping测试. (i) $NaYbSe_2$典型的AFM图片. (j, k) $NaYbSe_2$纳米片的高分辨透射图片(j)及对应的选区电子衍射图像(k). (l) $NaYbSe_2$纳米片的STEM图像和对应的元素面分布照片

Figure 1 (Color online) Synthesis and characterization of two-dimensional $NaYbSe_2$. (a) Crystal structure of $NaYbSe_2$. (b) Schematic diagram of CVD growth. (c) Optical photograph of $NaYbSe_2$. (d) XRD test. (e) The full width at half maximum (FWHM) of the (003) crystallographic plane diffraction peak of $NaYbSe_2$. (f) Raman test of $NaYbSe_2$ with different thicknesses. (g, h) Optical photographs of $NaYbSe_2$ and corresponding Raman mapping tests. (i) Typical AFM image of $NaYbSe_2$. (j, k) High-resolution TEM (HR-TEM) image of $NaYbSe_2$ nanosheets and the corresponding selected area electron diffraction (SAED) pattern. (l) STEM image of $NaYbSe_2$ nanosheets and corresponding elemental map distributions

后的R面蓝宝石衬底在光学显微镜下观察, 发现三角形纳米片均匀沉积在蓝宝石衬底上, 光学照片如图1(c)所示. 为了确定生长后得到的样品的物相结构, 首先进行了XRD测试. 结果如图1(d)所示, $NaYbSe_2$的(003)晶面衍射峰与标准卡片(PDF#51-1229)吻合, 且从图1(e)中得出(003)晶面的半峰宽接近0.1°, 说明通过CVD合成的$NaYbSe_2$具有良好的结晶性. 此外, R面蓝宝石的(012)和(024)晶面衍射峰强度明显高于$NaYbSe_2$的(003)晶面, 这归因于二维$NaYbSe_2$在R面蓝宝石表面的覆盖率较少且厚度较低. 拉曼光谱分析进一步证实了材料的成功合成. 如图1(f)所示, $NaYbSe_2$在126.26 cm^{-1}的E_g振动信号和171.78 cm^{-1}的A_{1g}振动信号, 峰位置和文献中报道的一致[35~37]. 随着$NaYbSe_2$厚度的增加, E_g和A_{1g}峰强度信号逐渐增强. 为评估材料均匀性, 在R面蓝宝石衬底上选取合适的目标区域(图1(g))进行了Raman面扫描分析, 图1(h)展示了E_g振动模式的强度空间分布图, 结果表明样品具有良好的结构均匀性. 借助AFM对$NaYbSe_2$的厚度进行表征, 典型的AFM图如图1(i)所示, 表明CVD制备的$NaYbSe_2$厚度平均值为49.7 nm, 其中一个典型三角形厚度约为43 nm. 透射电子显微镜是分析材料微观结构的有力工具, 图1(j)是$NaYbSe_2$纳米片的高分辨透射图像, 图中两个晶面间距为0.21 nm, 晶面夹角60°, 分别对应$(1\bar{2}0)$和$(2\bar{1}0)$晶面, 对应的选区电子衍射图像如图1(k)所示, 仅存在一套明亮衍射花样, 透射电子显微镜分析结果证实通过CVD合成的$NaYbSe_2$具有良好的单晶性. 对$NaYbSe_2$三角形纳米片进行元素面扫描分析, 扫描结果如图1(l)所示, $NaYbSe_2$边界清晰, Na、Yb和Se三种元素均匀分布在整个样品中. 以上透射电子显微镜表征结果充分证明, 通过CVD可以制备高质量$NaYbSe_2$单晶.

2.2 二维$NaYbSe_2$晶体生长调控

将生长温度均保持为900℃, 通过改变实验的生长时间, 系统地探究了二维$NaYbSe_2$纳米片的生长行为变化. 如图2(a)所示, 在20 min生长时间的条件下, $NaYbSe_2$晶体平均尺寸为5.1 μm, 呈现典型的三角形畴区形貌(图2(b)), 且具有较高的成核密度; 当生长时间延长至30 min时, $NaYbSe_2$纳米片仍呈现出三角形畴区形貌特征(图2(c)), 且三角形的尺寸增大, 平均尺寸达到13.4 μm. 生长20和30 min都表现为尖锐的边缘, 说明$NaYbSe_2$在延长生长时间下仍保持良好结晶性.

随后, 将生长时间均保持为20 min, 探究了不同温度对$NaYbSe_2$生长的影响. 在850℃生长温度下得到$NaYbSe_2$, 从光学显微镜上观察证实$NaYbSe_2$纳米片尺寸较小, 平均尺寸为1.5 μm, 且成核密度大(图2(d), (e)); 当生长温度升高至900℃时, 晶体平均尺寸增大至5.4 μm(图2(f)). 这一现象可归因于温度升高导致反应物质扩散速率加快, 反应速率增大, 从而促进晶体生

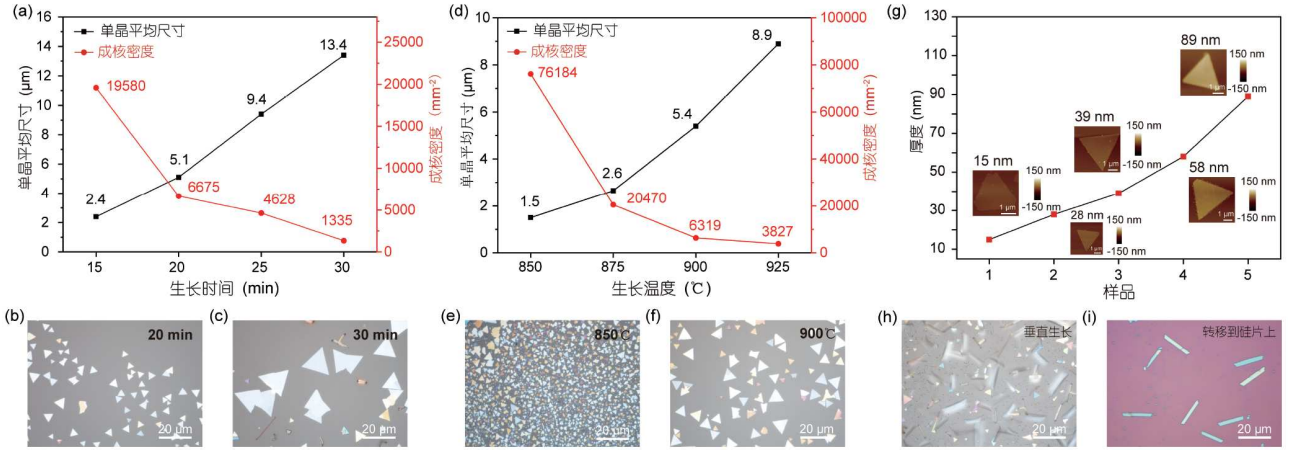


图 2 (网络版彩色)$NaYbSe_2$单晶生长调控. (a) $NaYbSe_2$单晶平均尺寸和成核密度随生长时间变化统计折线图. (b) 生长时间20 min. (c) 生长时间30 min. (d) $NaYbSe_2$单晶平均尺寸和成核密度随生长温度变化统计折线图. (e) 生长温度850℃. (f) 生长温度900℃. (g) $NaYbSe_2$不同厚度统计. (h) 垂直生长的$NaYbSe_2$. (i) 转移到硅片上的$NaYbSe_2$纳米片

Figure 2 (Color online) Regulation of single crystal growth of $NaYbSe_2$. (a) Statistical line chart of the average size and nucleation density of $NaYbSe_2$ single crystals with growth time. (b) Growth time: 20 min. (c) Growth time: 30 min. (d) Statistical line chart of the average size and nucleation density of $NaYbSe_2$ single crystals with growth temperature. (e) Growth temperature: 850°C. (f) Growth temperature: 900°C. (g) Statistics of different thicknesses of $NaYbSe_2$. (h) $NaYbSe_2$ grown vertically. (i) $NaYbSe_2$ nanosheets transferred to silicon wafers

长. 然而生长温度也不宜过高, 因为过高的温度会导致反应物质与活性前驱体在蓝宝石表面的脱附率升高, 不利于最终产物的形成.

通过精确调控生长参数, 实现了$NaYbSe_2$单晶厚度

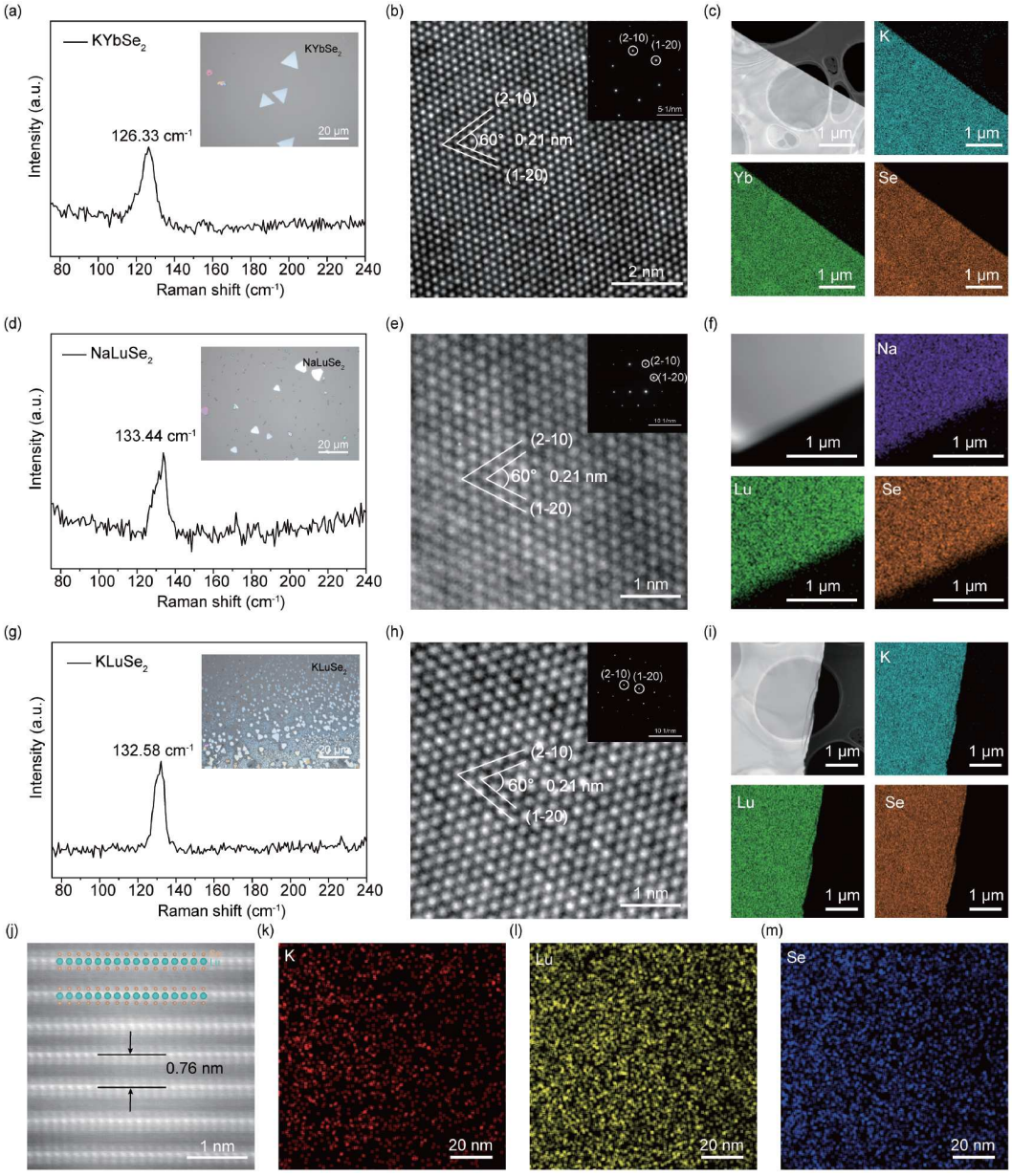


图 3 (网络版彩色)三种同类型新型二维材料合成及表征. (a) $KYbSe_2$的Raman光谱, 插图为其典型的光镜照片. (b) $KYbSe_2$的高分辨透射图片, 插图为对应的选区电子衍射图. (c) $KYbSe_2$纳米片的STEM图像和对应的元素面分布照片. (d) $NaLuSe_2$的Raman光谱, 插图为其典型的光镜照片. (e) $NaLuSe_2$的高分辨透射图片, 插图为对应的选区电子衍射图. (f) $NaLuSe_2$纳米片的STEM图像和对应的元素面分布照片. (g) $KLuSe_2$的Raman光谱, 插图为其典型的光镜照片. (h) $KLuSe_2$的高分辨透射图片, 插图为对应的选区电子衍射图. (i) $KLuSe_2$纳米片的STEM图像和对应的元素面分布照片. (j) $KLuSe_2$截面的HAADF-STEM图像和(k~m) K、Lu和Se元素分布图谱

Figure 3 (Color online) Synthesis and characterization of three novel 2D materials. (a) Raman spectrum of $KYbSe_2$, illustrated as a typical microscope image. (b) HR-TEM image of $KYbSe_2$ nanosheets. Inset: the corresponding SAED pattern of $KYbSe_2$. (c) STEM image of $KYbSe_2$ nanosheets and corresponding elemental map distributions. (d) Raman spectrum of $NaLuSe_2$, illustrated as a typical microscope image. (e) HR-TEM image of $NaLuSe_2$ nanosheets. Inset: the corresponding SAED pattern of $NaLuSe_2$. (f) STEM image of $NaLuSe_2$ nanosheets and corresponding elemental map distributions. (g) Raman spectrum of $KLuSe_2$, illustrated as a typical microscope image. (h) HR-TEM image of $KLuSe_2$ nanosheets. Inset: the corresponding SAED pattern of $KLuSe_2$. (i) STEM image of $KLuSe_2$ nanosheets and corresponding elemental map distributions. (j) HAADF-STEM images of $KLuSe_2$ cross-section and (k–m) K, Lu and Se element distribution maps

在15~89 nm范围内的可控生长(图2(g)). 特别值得注意的是, 在蓝宝石衬底与坩埚边缘接触区域观察到了独特的$NaYbSe_2$单晶垂直生长现象(图2(h). 将此类样品转移至硅片衬底后, 可观察到呈现梯形结构的$NaYbSe_2$晶体, 其最大边长超过20 μm(图2(i)). 这一发现为研究$NaYbSe_2$晶体的各向异性生长机制提供了重要线索.

2.3 二维$KYbSe_2$、$NaLuSe_2$和$KLuSe_2$晶体的合成及表征

基于$NaYbSe_2$的成功合成经验, 通过调控前驱体的组合, 进一步制备出$KYbSe_2$、$NaLuSe_2$和$KLuSe_2$三种二维化合物. 结构表征结果揭示了这些材料具有与$NaYbSe_2$相似的结构特征. 从图3(a)看出, $KYbSe_2$的Raman特征峰在126.33 cm^{-1}. 其高分辨透射电子显微镜图像和衍射图像如图3(b)所示, 和$NaYbSe_2$情况类似, $KYbSe_2$的$(1\bar{2}0)$晶面间距为0.21 nm, 且其元素面分布均匀, 如图3(c)所示, 证实了单晶$KYbSe_2$的成功合成. 同样地, 从图3(d)中可以看出$NaLuSe_2$单晶Raman特征峰在133.44 cm^{-1}, 其高分辨和衍射结果如图3(e)所示, $NaLuSe_2$的$(1\bar{2}0)$晶面间距为0.21 nm, 且其元素面分布均匀, 如图3(f)所示. $KLuSe_2$的Raman和TEM结果与上述情况相似, 不再赘述, 分别如图3(g)~(i)所示. 为深入研究这类材料的层间结构特性, 选取$KLuSe_2$进行截面分析. 通过聚焦离子束(focused ion beam, FIB)制备截面样品, 利用球差校正透射电子显微镜进行样品原子分辨成像分析, 实验观察到在$KLuSe_2$晶体中$[LuSe_2]^-$层间距离为0.76 nm, 与理论值吻合, 如图3(j)所示; 且K、Lu和Se三种元素分布均匀, 如图3(k)~(m)所示. 因此, 使用球差校正透射电子显微镜表征进一步证明了CVD合成二维$KLuSe_2$良好的单晶性, 并且其晶体结构符合理论预期.

3 结论

本研究通过化学气相沉积方法实现了$NaYbSe_2$、$NaLuSe_2$、$KYbSe_2$和$KLuSe_2$四种新型碱金属稀土硒化物的二维单晶纳米片合成. 通过对生长时间和温度等参数的调控, 获得了不同厚度和尺寸的单晶片层, 并结合Raman光谱、XRD、TEM和HAADF-STEM等多种手段系统地表征了其结构与形貌, 证明了其良好的单晶特性. 该成果表明, 碱金属稀土硒化物体系可以稳定存在于二维形态, 扩展了二维材料家族的范围. 未来的研究将主要围绕两个方面展开: 一方面, 通过优化生长条件和衬底类型, 有望进一步实现晶体取向的可控生长并提升厚度可控性, 获得尺寸更大的二维单晶; 另一方面, 二维$NaYbSe_2$及其同类化合物在低维极限下可能展现出丰富的新奇物理特性, 例如, 在低压条件下的绝缘态-金属态转变、与石墨烯等二维材料构筑异质结后界面耦合对量子态的调控, 以及低温输运和磁学测试中潜在的量子自旋液体行为和超导特性等. 这些方向的深入研究不仅有助于加深对稀土二维材料基础物性的理解, 也可能推动其在未来量子器件和自旋电子学中的应用.

参考文献

1 Novoselov K S, Geim A K, Morozov S V, et al. Electric field effect in atomically thin carbon films. Science, 2004, 306: 666–669

2 Ramos M, Gadea M, Mañas-Valero S, et al. Tunable, multifunctional opto-electrical response in multilayer $FePS_3$ /single-layer MoS_2 van der Waals p–n heterojunctions. Nanoscale Adv, 2024, 6: 1909–1916

3 Zhang Z, Zhao B, Shen D, et al. Synthesis of ultrathin 2D nonlayered α-MnSe nanosheets, MnSe/WS_2 heterojunction for high-performance photodetectors. Small Struct, 2021, 2: 2100028

4 Ghiasi T S, Kaverzin A A, Dismukes A H, et al. Electrical and thermal generation of spin currents by magnetic bilayer graphene. Nat Nanotechnol, 2021, 16: 788–794

5 Niu S, Cai J, Wang G. Two-dimensional MOS_2 for hydrogen evolution reaction catalysis: the electronic structure regulation. Nano Res, 2020, 14: 1985–2002

6 Ou H, Yan X, Wang C, et al. Chemical vapor deposition and applications of vertical graphene: progress and prospects (in Chinese). Chin Sci Bull, 2024, 69: 4748–4762 [区昊雄, 颜鑫承, 王超, 等. 站立式石墨烯的化学气相沉积及其应用: 现状与展望. 科学通报, 2024, 69: 4748–4762]

7 Zeng F, Bai J, Zhang X, et al. Progress on the growth of two-dimensional single crystals on insulating substrates (in Chinese). Chin Sci Bull, 2024, 69: 3887–3899 [曾凡凯, 白金霞, 张晓闻, 等. 绝缘衬底上二维单晶材料制备研究进展. 科学通报, 2024, 69: 3887–3899]

8 Jang A R, Hong S, Hyun C, et al. Wafer-scale and wrinkle-free epitaxial growth of single-orientated multilayer hexagonal boron nitride on sapphire. Nano Lett, 2016, 16: 3360–3366

9 Kubota Y, Watanabe K, Tsuda O, et al. Deep ultraviolet light-emitting hexagonal boron nitride synthesized at atmospheric pressure. Science, 2007,

317: 932–934
10 Li J, Yang X, Liu Y, et al. General synthesis of two-dimensional van der Waals heterostructure arrays. Nature, 2020, 579: 368–374
11 Yang X, Li J, Liang T, et al. Antibacterial activity of two-dimensional MoS_2 sheets. Nanoscale, 2014, 6: 10126–10133
12 Zhang Y, Yao Y, Sendeku M G, et al. Recent progress in CVD growth of 2D transition metal dichalcogenides and related heterostructures. Adv Mater, 2019, 31: 1901694
13 Cheema S S, Shanker N, Wang L C, et al. Ultrathin ferroic HfO_2–ZrO_2 superlattice gate stack for advanced transistors. Nature, 2022, 604: 65–71
14 Feng X, Cheng R, Yin L, et al. Two-dimensional oxide crystals for device applications: challenges and opportunities. Adv Mater, 2023, 36: 2304708
15 Ma R, Sasaki T. Two-dimensional oxide and hydroxide nanosheets: controllable high-quality exfoliation, molecular assembly, and exploration of functionality. Acc Chem Res, 2014, 48: 136–143
16 Anderson P W. Resonating valence bonds: a new kind of insulator? Mater Res Bull, 1973, 8: 153–160
17 Anderson P W. The resonating valence bond state in La_2CuO_4 and superconductivity. Science, 1987, 235: 1196–1198
18 Anderson P W, Baskaran G, Zou Z, et al. Resonating–valence-bond theory of phase transitions and superconductivity in La_2CuO_4-based compounds. Phys Rev Lett, 1987, 58: 2790–2793
19 Jia Y, Gong C, Li Z, et al. Pressure induced insulator to metal transition in quantum spin liquid candidate $NaYbS_2$. Chin Phys B, 2023, 32: 096201
20 Jia Y T, Gong C S, Liu Y X, et al. Mott transition and superconductivity in quantum spin liquid candidate $NaYbSe_2$. Chin Phys Lett, 2020, 37: 097404
21 Wang H, Shi L, Huyan S, et al. Pressure-induced insulator-to-metal transition in the quantum spin liquid candidate lithium ytterbium diselenide. Cell Rep Phys Sci, 2024, 5: 101989
22 Xie M, Zhuo W, Cai Y, et al. Rare-earth chalcogenides: an inspiring playground for exploring frustrated magnetism. Chin Phys Lett, 2024, 41: 117505
23 Guo L, Yang X F, Cheng E J, 等. Pressure-induced superconductivity in triangular lattice spin liquid candidate $NaYbSe_2$ (in Chinese). Acta Phys Sin, 2023, 72: 157401 [郭琳, 杨小帆, 程二建, 等. 三角晶格自旋液体候选材料$NaYbSe_2$在高压下的超导转变. 物理学报, 2023, 72: 157401]
24 Xu Y, Sheng Y, Yang Y. Mechanism of the insulator-to-metal transition and superconductivity in the spin liquid candidate $NaYbSe_2$ under pressure. npj Quantum Mater, 2022, 7: 21
25 Zhu Z, Pan B, Nie L, et al. Fluctuating magnetic droplets immersed in a sea of quantum spin liquid. Innovation, 2023, 4: 100459
26 Bordelon M M, Kenney E, Liu C, et al. Field-tunable quantum disordered ground state in the triangular-lattice antiferromagnet $NaYbO_2$. Nat Phys, 2019, 15: 1058–1064
27 Liu W, Zhang Z, Ji J, et al. Rare-earth chalcogenides: a large family of triangular lattice spin liquid candidates. Chin Phys Lett, 2018, 35: 117501
28 Scheie A O, Ghioldi E A, Xing J, et al. Proximate spin liquid and fractionalization in the triangular antiferromagnet $KYbSe_2$. Nat Phys, 2023, 20: 74–81
29 Ma H, Wan Z, Li J, et al. Phase-tunable synthesis of ultrathin layered tetragonal CoSe and nonlayered hexagonal CoSe nanoplates. Adv Mater, 2019, 31: 1900901
30 Zhao Z, Zhou J, Liu L, et al. Two-dimensional room-temperature magnetic nonstoichiometric Fe_7Se_8 nanocrystals: controllable synthesis and magnetic behavior. Nano Lett, 2022, 22: 1242–1250
31 Zhang Z, Niu J, Yang P, et al. Van der Waals epitaxial growth of 2D metallic vanadium diselenide single crystals and their extra-high electrical conductivity. Adv Mater, 2017, 29: 1702359
32 Ge J, Luo T, Lin Z, et al. Magnetic moments induced by atomic vacancies in transition metal dichalcogenide flakes. Adv Mater, 2020, 33: 2005465
33 Zou J, Yang Y, Hu D, et al. Controlled growth of ultrathin ferromagnetic β-MnSe semiconductor. SmartMat, 2022, 3: 482–490
34 Dai P L, Zhang G, Xie Y, et al. Spinon fermi surface spin liquid in a triangular lattice antiferromagnet $NaYbSe_2$. Phys Rev X, 2021, 11: 021044
35 Pai Y, Marvinney C E, Pokharel G, et al. Angular-momentum transfer mediated by a vibronic-bound-state. Adv Sci, 2023, 11: 2304698
36 Pritchard Cairns L, Day R, Haley S, et al. Tracking the evolution from isolated dimers to many-body entanglement in $NaLu_xYb_{1-x}Se_2$. Phys Rev B, 2022, 106: 024404
37 Zhang Z, Ma X, Li J, et al. Crystalline electric field excitations in the quantum spin liquid candidate $NaYbSe_2$. Phys Rev B, 2021, 103: 035144

Summary for “化学气相沉积法制备二维碱金属稀土硒化物单晶”

Chemical vapor deposition growth of two-dimensional alkali-metal-based rare-earth selenide single crystals

Jialin Zhang[1], Xiaohui Chen[2], Li Lin[2*] & Chunhu Li[1*]

[1] *Key Laboratory of Marine Chemistry Theory and Technology, Ministry of Education, College of Chemistry and Chemical Engineering, Ocean University of China, Qingdao 266100, China*
[2] *School of Materials Science and Engineering, Peking University, Beijing 100871, China*
* Corresponding authors, E-mail: linli-cnc@pku.edu.cn; lichunhu@ouc.edu.cn

In recent years, two-dimensional materials have attracted extensive attention due to their excellent physical and chemical properties at extremely thin thicknesses. Two-dimensional rare earth materials, owing to the unique localized 4f electrons of rare earth elements and strong magnetic anisotropy, can be used to construct highly stable nano-magnets, demonstrating significant application potential in spintronic devices. Moreover, their interface effects can be utilized to modulate the superconducting properties of adjacent systems in the field of superconductivity, providing a platform for the investigation of novel superconducting states. $NaYbSe_2$ has attracted much attention because of its use as a candidate material for quantum spin liquids and its superconductivity at high pressures. In 1973, Anderson proposed the novel quantum state of quantum spin liquids, which garnered significant attention. Subsequently, in 1987, Anderson and others further suggested the theoretical possibility of achieving high-temperature superconductivity through doping of quantum spin liquids. This theory has prompted researchers to conduct in-depth studies on the transition of $NaYbSe_2$ from an insulating state to a metallic and superconducting state.

Currently, the preparation method of $NaYbSe_2$ is as follows: it is obtained by growing using metallic Yb, Se, and NaCl as flux, and the synthesized $NaYbSe_2$ is in the form of bulk material. However, the systematic preparation of two-dimensional $NaYbSe_2$ remains unattainable. In this study, the two-dimensional $NaYbSe_2$ was successfully prepared on R-plane sapphire by chemical vapor deposition, with NaCl, Yb, and Se as precursors and hydrogen and argon as carrier gases. Raman characterization shows that the peak intensities of Eg and A1g modes gradually increase with the increase of $NaYbSe_2$ thickness. X-ray diffraction (XRD) analysis of the characteristic (003) peak of $NaYbSe_2$ reveals a narrow full width at half maximum (FWHM), confirming the good single-crystal properties of the material. By regulating growth parameters, nanosheets with thicknesses ranging from 15 to 89 nm can be prepared, with sizes reaching up to 20 μm. Additionally, vertically grown structures of $NaYbSe_2$ were observed at the substrate edges; this unique growth behavior is beneficial for the transfer of this material, thereby providing a material foundation for the subsequent construction of three-dimensional devices. Transmission electron microscopy (TEM) analysis has confirmed that $NaYbSe_2$ nanosheets exhibit good single-crystal characteristics at the microscopic scale for the first time. This preparation method can be further extended to the synthesis of a series of two-dimensional single-crystal thin sheets, such as $NaLuSe_2$, $KYbSe_2$, and $KLuSe_2$, by changing the type of precursor. At the same time, the high-angle annular dark-field scanning transmission electron microscopy (HAADF-STEM) image revealed that the interlayer distance of $KLuSe_2$ was 0.76 nm. As a Mott insulator, $NaYbSe_2$ could be used to regulate the critical conditions of its superconducting phase transition by constructing heterojunctions with other two-dimensional materials at the nanoscale. Therefore, the controllable preparation and excellent single-crystal properties of 2D materials such as $NaYbSe_2$ will promote the study of their physical properties and related applications in spin devices.

two-dimensional materials, chemical vapor deposition, alkali-metal-based rare-earth selenides, single crystal

doi: 10.1360/CSB-2025-5357